PERGAMON

International Journal of Solids and Structures 38 (2001) 5063–5079

INTERNATIONAL JOURNAL OF SOLIDS and STRUCTURES

www.elsevier.com/locate/ijsolstr

The role of crack rate dependence in the long-term behaviour of cementitious materials

G.P.A.G. van Zijl [a,*], R. de Borst [b], J.G. Rots [a]

[a] *Faculty of Architecture, Delft University of Technology, P.O. Box 5043, Berlageweg 1, 2600 GA Delft, CR, Netherlands*

[b] *Koiter Institute Delft/Faculty of Aerospace Engineering, Delft University of Technology, P.O. Box 5058, Berlageweg 1, 2600 GB Delft, CR, Netherlands*

Received 8 June 2000

Abstract

The main purpose of this paper is to bring forth new evidence that the introduction of cracking rate terms in the analysis of quasi-static localisation in cementitious materials is not merely a numerical artefact. It has been introduced in the past to regularise the continuum description of localisation. In this paper it is demonstrated that the rate terms also have a physical role. They introduce the correct time scale in quasi-static cracking. Crack rate models are presented in a finite element setting, which combines linear visco-elasticity and anisotropic Rankine plasticity. The introduction of a cracking viscosity is shown to regularise the cracking in a shrinking masonry wall, which is externally restrained by the foundation. Subsequently, the physical role of the rate terms is brought out by the analysis of three-point bending creep failure experiments on concrete. If the crack rate dependence is ignored, the global load–deformation response can be represented, but the time to failure under the sustained load is overestimated by several orders of magnitude. Upon introduction of crack rate dependence, which is characterised by the inverse analysis of separate, material characterisation experiments, the correct, i.e. the experimentally observed time to failure is calculated.

Keywords: Concrete; Masonry; Localisation; Regularisation; Crack rate dependence; Creep

1. Introduction

For some time it has been known that by adding a rate term to the cracking stress, the continuum description of localisation can be regularised in dynamic analyses (Sluys, 1992; Wang, 1997). The loss of hyperbolicity of the governing differential equations upon localisation is prevented and the ensuing numerical convergence difficulty, or mesh dependent numerical response is avoided. These symptoms also occur in unregularised quasi-static localisation analyses, triggered by the loss of the elliptic character of the governing equations. De Borst et al. (1993) have shown that by considering a cracking viscosity, the

* Corresponding author. Tel.: +31-15-2784367; fax: +31-15-2784178.
E-mail address: g.p.a.g.vanzijl@bk.tudelft.nl (G.P.A.G. van Zijl).

0020-7683/01/$ - see front matter
PII: S0020-7683(00)00338-3

governing differential equation of a quasi-static problem becomes parabolic upon localisation, instead of hyperbolic and remains well posed.

It is not justifiable to introduce such regularising rate terms as numerical artefacts. Indeed, the behaviour of cementitious materials is time/rate dependent, governed by its continuously changing micro-structure and the ever-present moisture in the pores. Experimental evidence exists that the loading rate does not influence the structural response of cementitious materials only in the dynamic range, but that structural resistance is also enhanced by an increase in the loading rate within the quasi-static range (Zhou, 1992; Bažant and Gettu, 1992). In the quasi-static range the creep processes play an important role and can, by itself, describe a range in structural resistance. By the (creep) process of debonding and rebonding of micro-structural particles, enhanced by the disruptive moisture flux between micro-pores and macro-pores (Powers, 1968; Bažant and Chern, 1985), a degradation is caused, which can limit the life expectancy of a structure.

It is likely that a different mechanism acts in the localised fracture process zone (FPZ) and governs the crack propagation velocity, especially in the final stages of crack opening (Bažant and Xiang, 1997). Wu and Bažant (1993) postulate that the activation energy-controlled process of bond ruptures in the FPZ governs the cracking rate. They have shown that the crack mouth opening rate (CMOR) model, which they derived from this postulation, can capture the observed strength increase with loading rate in a wide range of quasi-static loading rates, which is not possible if only creep is considered. In this paper the focus is on the time scale involved in quasi-static creep failure, which presents more evidence of such an additional source of rate dependence in the FPZ.

A finite element model is presented, which incorporates both sources of time dependence in cementitious materials. Linear visco-elasticity is employed to model the bulk creep, justified by the linearity of tensile creep isochrones. It is combined with a rate-dependent crack model, which is an extension of an anisotropic Rankine plasticity model (Lourenço, 1996) to include the cracking rate term(s). After an outline of the model, the regularising role of the CMOR dependence is demonstrated in the analysis of restrained shrinking masonry walls. Subsequently, the three-point bending creep experiments on concrete beams by Zhou (1992) are analysed, in which the physical role of the CMOR dependence in capturing the real time scale is demonstrated.

2. Crack rate dependence

Wu and Bažant (1993) postulate that the activation energy-controlled process of bond ruptures in the FPZ governs the cracking rate. Thus, the starting point of continuum plasticity, continuum damage mechanics and creep models, namely the stochastic nature of the thermally activated particle vibrations, which lead to bond rupture and cause micro-structural changes such as dislocations, crystalline slip, nucleation and micro-cracking, is revisited. It is argued that the bond ruptures occur at a finite rate, governed by the Maxwell–Boltzmann distribution of exceedence of the activation energy, which is the energy level which has to be exceeded to cause a bond between particles to rupture. Along this route the following expression for the crack opening rate $\dot{w}$ can be derived (Wu and Bažant, 1993) for isothermal conditions:

$$\dot{w} = \dot{w}_{\mathrm{r}} \sinh\left[\frac{\sigma - \sigma_t(w)}{k_0[\sigma_t(w) + k_1 f_t]}\right], \tag{1}$$

where $\dot{w}_{\mathrm{r}}$ is a constant, reference crack opening velocity and $\sigma_t(w)$ describes the strength degradation with an infinitely low crack opening velocity. The model parameter k_0 is estimated to be in the range 0.01–0.08 from the knowledge that for a 10^4-fold increase of the loading rate a 25% increase in peak strength is found experimentally. The model parameter k_1 is an offset factor to prevent the denominator in Eq. (1) from

becoming zero. By approximating the crack opening displacement $w = l_b\kappa$, with l_b the crack bandwidth and κ the crack strain, Eq. (1) can be rewritten as

$$\sigma = \sigma_t(\kappa)\left[1 + k_0 \sinh^{-1}\left(\frac{\dot{\kappa}}{\dot{\kappa}_r}\right)\right] + k_0 k_1 f_t \sinh^{-1}\left(\frac{\dot{\kappa}}{\dot{\kappa}_r}\right). \tag{2}$$

A justified criticism of this model is that the micro-structural mechanism is hardly distinguishable from the one used to derive the bulk creep description. It is widely agreed that the time/rate effects in cementitious materials are caused by the moisture and its migration in the material. A simple, alternative approach is, therefore, to consider the cracking process to be viscous and to describe this process with a viscosity term which acts only in the FPZ, following Sluys (1992) and De Borst et al. (1993). Thereby, the cracking stress is supplemented with a rate term

$$\sigma = \sigma_t(\kappa)\left[1 + \frac{m}{f_t}\dot{\kappa}\right], \tag{3}$$

where m is the cracking viscosity. The rate term is degraded with increasing crack width to avoid a residual strength. This one-parameter model is of a similar form as the three-parameter model of Eq. (2), except for the residual term.

3. Computational model

The crack rate models described in Section 2 have been incorporated in a computational framework, which combines linear visco-elasticity and continuum plasticity. The simulation of the bulk creep with linear visco-elasticity is justified by the approximately linear tensile creep isochrones of cementitious materials like concrete and masonry. The continuum, softening plasticity formulation, which captures crack initiation and propagation, does not reflect on the actual, quasi-brittle material behaviour, but provides a convenient macroscopic modelling framework. Constitutive laws based in continuum plasticity have been shown to model cracking in concrete (Feenstra, 1993; de Borst et al., 1994) and in masonry (Lourenço, 1996) with reasonable accuracy.

The combined constitutive law is expressed in rate form as

$$\dot{\boldsymbol{\sigma}} = \boldsymbol{D}^{ve}\left(\dot{\boldsymbol{\varepsilon}} - \dot{\boldsymbol{\varepsilon}}_{cr} - \dot{\boldsymbol{\varepsilon}}_0\right) + \boldsymbol{\Sigma}. \tag{4}$$

where $\boldsymbol{D}^{ve}$ is an equivalent, time-dependent stiffness modulus, $\boldsymbol{\Sigma}$ is a viscous stress term which accounts for the history, $\dot{\boldsymbol{\varepsilon}}_{cr}$ is the cracking strain rate and $\dot{\boldsymbol{\varepsilon}}_0$ represents the dimensional change due to hygral and thermal shrinkage. The latter contribution may be stress dependent. To derive Eq. (4) it has been assumed that the strain rate can be decomposed as follows:

$$\dot{\boldsymbol{\varepsilon}} = \dot{\boldsymbol{\varepsilon}}_{ve} + \dot{\boldsymbol{\varepsilon}}_{cr} + \dot{\boldsymbol{\varepsilon}}_0, \tag{5}$$

where $\boldsymbol{\varepsilon}_{ve}$ is the visco-elastic strain.

The rate Eq. (4) can be integrated with a linear scheme, which produces the stress increment in the time increment Δt

$$\Delta\boldsymbol{\sigma} = \boldsymbol{D}^{ve}(\Delta\boldsymbol{\varepsilon} - \Delta\boldsymbol{\varepsilon}_{cr} - \Delta\boldsymbol{\varepsilon}_0) + {}^t\tilde{\boldsymbol{\sigma}}, \tag{6}$$

where

$$\begin{aligned} \boldsymbol{D}^{\mathrm{ve}} &= \left[E_0(t^*) + \sum_{n=1}^{N}\left(1 - \mathrm{e}^{-\Delta t/\zeta_n}\right)\frac{E_n(t^*)}{\Delta t/\zeta_n}\right]\boldsymbol{D}, \\ {}^{t}\tilde{\boldsymbol{\sigma}} &= -\sum_{n=1}^{N}\left(1 - \mathrm{e}^{-\Delta t/\zeta_n}\right){}^{t}\boldsymbol{\sigma}_n. \end{aligned} \tag{7}$$

In this model an ageing Maxwell chain can be identified, with time dependent element stiffnesses $E_n(t)$ and viscosities $\eta_n = E_n\zeta_n$, ζ_n being the relaxation time of chain element n. The stress vector ${}^{t}\boldsymbol{\sigma}_n$ contains the stress components in chain element n at the end of the previous time step, i.e. at time t. Note that the parameters are assumed to be constant in each time interval and are evaluated at a time $t \leqslant t^* \leqslant t + \Delta t$. $\boldsymbol{D}$ is a dimensionless matrix which is dependent on Poisson's ratio v (de Borst et al., 1994; van Zijl, 2000).

The crack strain increment follows from the plastic flow

$$\Delta\boldsymbol{\varepsilon}_{\mathrm{cr}} = \Delta\kappa\frac{\partial g}{\partial\boldsymbol{\sigma}}, \tag{8}$$

with $g = g(\boldsymbol{\sigma}, \kappa)$ the plastic potential function. The stress is limited by the yield function

$$f(\boldsymbol{\sigma}, \kappa) \leqslant 0. \tag{9}$$

An anisotropic Rankine yield function is appropriate for the cohesive material of interest. It can be formulated in plane stress as (Lourenço, 1996)

$$f = \frac{(\sigma_x - \sigma_{tx}) + (\sigma_y - \sigma_{ty})}{2} + \sqrt{\left(\frac{(\sigma_x - \sigma_{tx}) - (\sigma_y - \sigma_{ty})}{2}\right)^2 + \alpha\tau_{xy}^2}, \tag{10}$$

where α controls the shear stress contribution to failure. The potential function has been chosen as

$$\mathrm{g} = f\,|_{\alpha=1}\,. \tag{11}$$

The cracking stresses in the orthogonal directions are given by

$$\sigma_{tx} = f_{tx}\exp\left(-\frac{f_{tx}}{g_{fx}}\kappa\right), \qquad \sigma_{ty} = f_{ty}\exp\left(-\frac{f_{ty}}{g_{fy}}\kappa\right). \tag{12}$$

The tensile strengths are denoted by f_{tx} and f_{ty}, while g_{fx} and g_{fy} are the fracture energies in the orthogonal directions. To add the rate dependence elaborated in Section 2, the cracking strength function can be supplemented with rate terms. With the three-parameter model of Eq. (2) the cracking stress reads

$$\begin{aligned} \sigma_{tx} &= f_{tx}\exp\left(-\frac{f_{tx}}{g_{fx}}\kappa\right)\left[1 + k_0\sinh^{-1}\left(\frac{\dot{\kappa}}{\dot{\kappa}_{\mathrm{r}}}\right)\right] + k_0k_1f_{tx}\sinh^{-1}\left(\frac{\dot{\kappa}}{\dot{\kappa}_{\mathrm{r}}}\right), \\ \sigma_{ty} &= f_{ty}\exp\left(-\frac{f_{ty}}{g_{fy}}\kappa\right)\left[1 + k_0\sinh^{-1}\left(\frac{\dot{\kappa}}{\dot{\kappa}_{\mathrm{r}}}\right)\right] + k_0k_1f_{ty}\sinh^{-1}\left(\frac{\dot{\kappa}}{\dot{\kappa}_{\mathrm{r}}}\right). \end{aligned} \tag{13}$$

For the simple cracking viscosity (Eq. (3)) the cracking stress is given by

$$\sigma_{tx} = \left(f_{tx} + m\dot{\kappa}\right)\exp\left(-\frac{f_{tx}}{g_{fx}}\kappa\right), \qquad \sigma_{ty} = \left(f_{ty} + m\dot{\kappa}\right)\exp\left(-\frac{f_{ty}}{g_{fy}}\kappa\right). \tag{14}$$

4. Regularisation of the continuum description of localisation

The regularisation of quasi-static fracture by the CMOR rate model is demonstrated next. It has been demonstrated recently (van Zijl, 2000) that the three-parameter CMOR model (Eq. (2)) regularises.

However, it does so only in a limited range of the reference cracking rate, due to the strong logarithmic type inverse hyperbolic operator (Eq. (2)). In this section the cracking viscosity model (Eq. (3)) is employed. A masonry wall subjected to drying, but restrained at the base by a non-shrinking foundation is analysed. This choice is motivated by the wide-spread occurrence of unsightly and, in some cases, serviceability impairing cracks in masonry buildings.

4.1. Modelling approach

The single leaf wall shown in Fig. 1 is modelled as a two-dimensional, homogeneous plane. A plane stress formulation is adopted, which captures the response to mechanical in-plane actions accurately (Lourenço, 1996; Rots, 1997). By employing the anisotropic Rankine yield criterion, the different strengths and softening characteristics of masonry in the directions normal and parallel to the bed joints are accounted for.

Symmetry is assumed, which allows only one half of the wall to be modelled. Both the wall and the foundation beam are modelled as homogeneous continua with three-noded triangular, or four-noded quadrilateral elements. Interface elements are employed to model the separation and slip between the foundation and the wall. They obey a Coulomb-friction material law (Lourenço, 1996; van Zijl, 2000) with adhesive strength 0.6 $\mathrm{N\,mm^{-2}}$ and a friction coefficient and a dilatancy coefficient 0.75 and 0.2 respectively. Exponential adhesion softening with shear-slipping is assumed, with a fracture energy 0.1 $\mathrm{N\,mm^{-1}}$. The Coulomb-friction criterion is limited by a tension cut-off at 0.3 $\mathrm{N\,mm^{-2}}$ and subsequent exponential softening with crack opening, governed by a fracture energy 0.02 $\mathrm{N\,mm^{-1}}$.

The wall has an initial elasticity modulus of 5000 $\mathrm{N\,mm^{-2}}$ and a constant Poisson's ratio of 0.2. The Rankine model parameters are $\alpha = 1$, $f_{tx} = 0.42\ \mathrm{N\,mm^{-2}}$, with x parallel to the bed/horizontal joints, $f_{ty} = 0.22\ \mathrm{N\,mm^{-2}}$, $g_{ftx} = 0.00011\ \mathrm{N\,mm^{-2}}$ and $g_{fty} = 0.000055\ \mathrm{N\,mm^{-2}}$. These parameter values represent a typical calcium silicate masonry. The foundation beam has a Young's modulus of 30 000 $\mathrm{N\,mm^{-2}}$ and a Poisson's ratio of 0.2. It is assumed not to shrink, creep, or crack. A geometrical imperfection has been modelled at the central (2×)120 mm wide column of the masonry wall by reducing the thickness by 5%. This has been done to avoid the approximately homogeneous stress state in the central area, which is a result of the continuum approach. The imperfection fixes the primary crack location. The objective is now

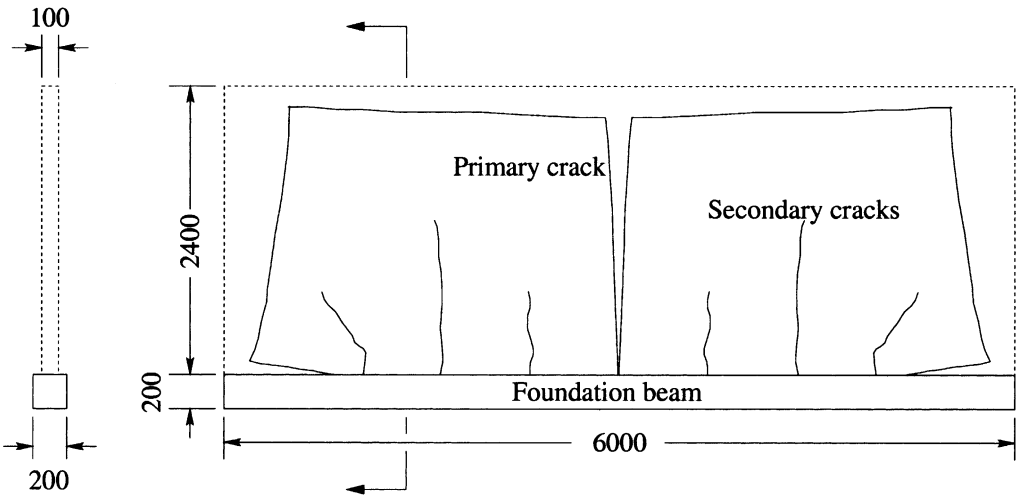

Fig. 1. Observed crack pattern in base-restrained shrinkage wall. Dimensions in mm.

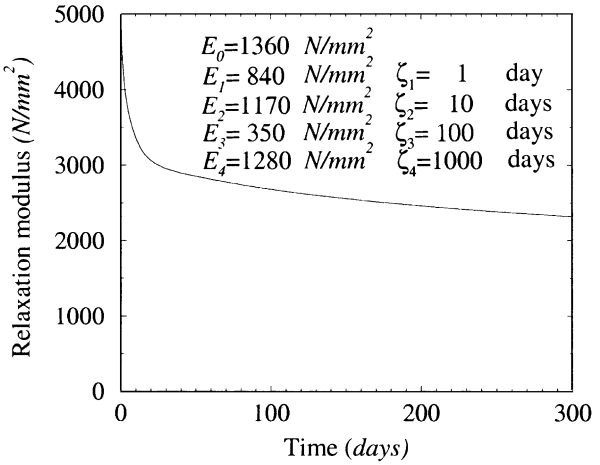

Fig. 2. Relaxation modulus for calcium silicate masonry.

to study the objectivity with which the proposed model predicts the position and orientation of other, non-seeded cracks in the wall.

A relaxation modulus typical for calcium silicate masonry, which was obtained from creep measurement data (van der Pluijm and Wubs, 1996) is employed. It is represented by a five-element Maxwell chain, of which the element stiffnesses and relaxation times are shown in Fig. 2. Despite evidence of masonry creep ageing (Shrive et al., 1997) it is not considered for lack of data.

The own weight of the wall is considered, with the masonry density 1800 $\mathrm{kg\,m^{-3}}$ and the foundation concrete density 2400 $\mathrm{kg\,m^{-3}}$. A further vertical load of eight times the own weight is considered to bear on top of the wall. The wall dimensions are shown in Fig. 1.

Spatially uniform, isotropic, stress-independent drying shrinkage is assumed, expressed by the shrinkage strain evolution

$$\varepsilon_{\mathrm{s}} = \alpha_{\mathrm{s}}(h_{\mathrm{E}} - h_0)\left(1 - \exp\left(-2\frac{\beta t}{cL_{\mathrm{d}}}\right)\right) \tag{15}$$

where α_{s} is the shrinkage coefficient, chosen here as 0.001, h_{E} is the environmental humidity, assumed to be uniform and constant at 0.6, h_0 is the initial, macroscopic pore humidity of the masonry, assumed to be 1.0 uniformly, β is the surface convection/film coefficient, taken as 5 $\mathrm{mm\,day^{-1}}$, c is the moisture absorption capacity, taken as 1.0 and L_{d} the wall thickness. This evolution is shown in Fig. 3.

4.2. Base-restrained shrinkage response

In the analysis, the own weight and top vertical load are applied in an initial step. Subsequently, the wall is subjected to the shrinkage evolution of Fig. 3, while accounting for creep and cracking. Firstly, the rate term is not activated, but instead, the crack band type fracture energy dissipation regularisation (Bažant and Oh, 1983) is employed, by relating the element size to the crack bandwidth. Fig. 4a shows the computed response in terms of the width of the primary crack versus the shrinkage strain level. The wall behaves elastically up to a shrinkage of approximately 0.13 $\mathrm{mm\,m^{-1}}$. Then the primary crack is initiated at the bottom centre of the wall. Subsequently the primary crack propagates upward and widens, while also secondary cracking starts. With the triangular element mesh, the primary crack dominates, but with the quadrilateral mesh, this crack is arrested when the secondary crack propagates. Also, different spacing as

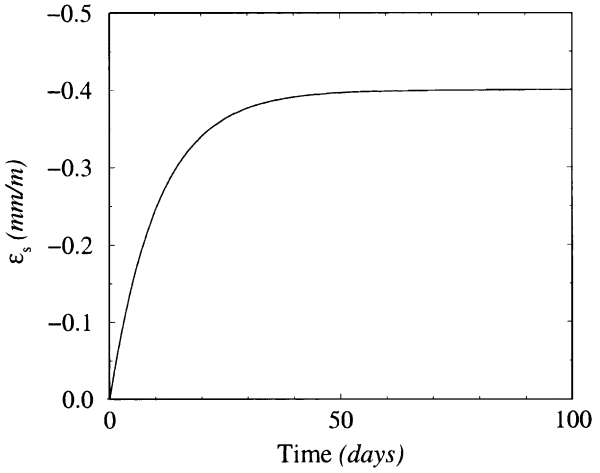

Fig. 3. Shrinkage strain evolution.

well as orientation of the cracks are predicted by the different meshes (Fig. 4). It is clear that the model produces mesh dependent crack spacing and orientation when the crack rate independence is not activated.

Next, the simple cracking viscosity model (Eq. (14)) is activated. No direct way of determining the cracking rate parameter exists. Instead, a cracking viscosity is sought which modifies the rate-independent response sufficiently at the acting loading/shrinkage rate to regularise the localisation process. For this purpose a uniaxially restrained masonry specimen has been analysed, with different cracking viscosities m. For each value of m it has been subjected to different, constant shrinkage rates. Fig. 5 shows the responses for $m = 2000\ \mathrm{N\,day\,mm^{-2}}$. A shrinkage rate of $\dot{\varepsilon}_s = 2 \times 10^{-5}\,\mathrm{day^{-1}}$ is representative of the shrinkage rate during the first 10 days of the shrinkage evolution in the wall (Eq. (15)). It can be seen that the viscosity $m = 2000\ \mathrm{N\,day\,mm^{-2}}$ produces a slight increase in strength at $\dot{\varepsilon}_s = 2 \times 10^{-5}\,\mathrm{day^{-1}}$ compared to the rate-independent response. This is the minimum requirement for the rate effect to regularise the base-restrained shrinking wall response. Furthermore, a 50% increase in peak strength is achieved by a 10^4-fold increase in the shrinkage rate, from $\dot{\varepsilon}_s = 2 \times 10^{-8}\,\mathrm{day^{-1}}$ to $\dot{\varepsilon}_s = 2 \times 10^{-4}\,\mathrm{day^{-1}}$. Note that the former low rate response coincides with the rate-independent response ($m = 0$). This strength increase is in agreement with experimental evidence. However, there is an excessive strength increase beyond this loading range ($\varepsilon_s > 2 \times 10^{-4}\,\mathrm{day^{-1}}$). This does not mean that the viscosity is invalid, but rather that either a rate-dependent viscosity should be used, or that a logarithmic-type formulation such as Eq. (13) should be considered for application in loading ranges beyond the current loading range. The cracking rate viscosity $m = 2000\ \mathrm{N\,day\,mm^{-2}}$ is employed for the wall analysis.

As shown in Fig. 6, the crack evolution, spacing and orientation are now predicted objectively by various element discretisations.

5. The physical role of CMOR dependence

To rid the inclusion of rate terms into the quasi-static formulation of the stigma of an artificial regularisation trick, the physical role of the CMOR dependence is studied next. It has been shown by Wu and Bažant (1993) that such a rate dependence enables the description of the loading rate dependence of concrete in a wide range of quasi-static loading rates. As in this model (Section 3) they included two sources of time dependence, namely the bulk creep as well as the CMOR formulation of Eq. (2). Although they did

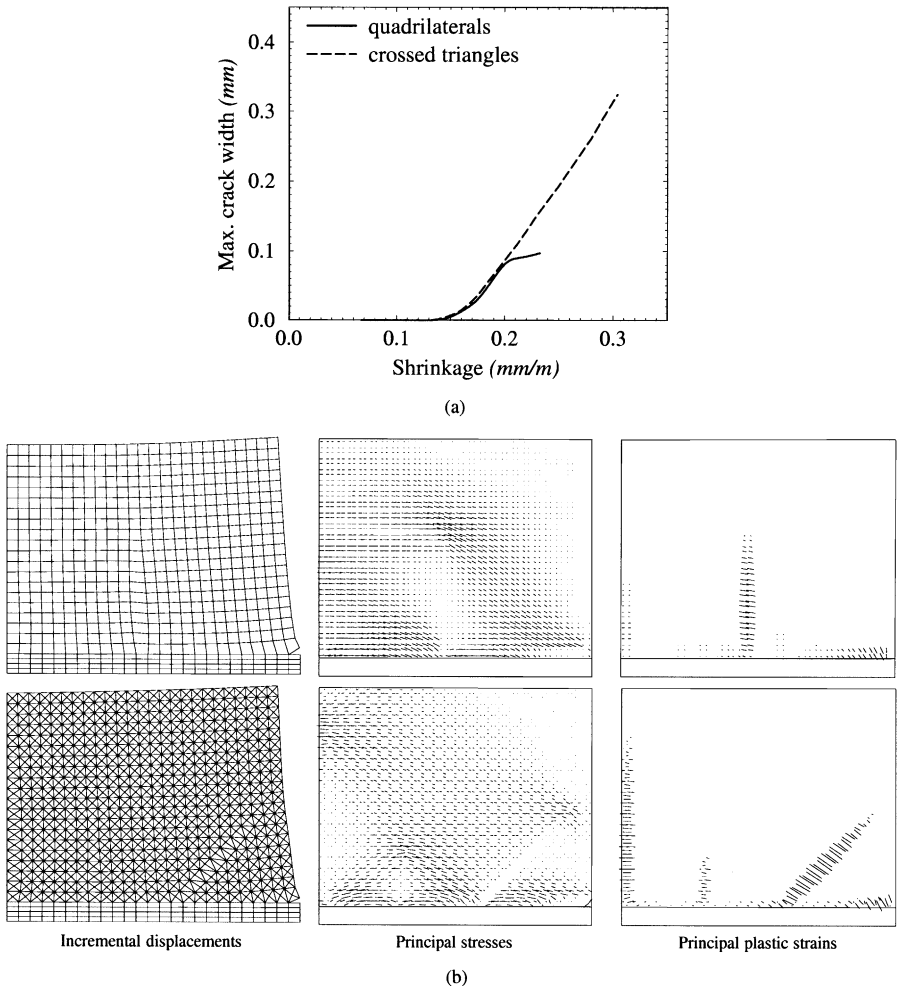

Fig. 4. Unregularised base-restrained shrinking masonry wall crack pattern. (a) Primary crack width evolution. (b) Deformation, maximum principal stresses and principal plastic strains.

not discuss it, it is clear that without the latter, i.e. with only bulk creep considered, the experimental loading rate dependence cannot be reproduced. Here, another role of the cracking velocity is brought out by a process of elimination. Three-point bending displacement-controlled, as well as creep experiments by Zhou (1992) are analysed with both sources of time dependence first, and subsequently with only bulk creep activated. From the displacement-controlled experiments the total load–deformation response was obtained. For a given loading rate this response can be reproduced with either one, or with both sources of time-dependence activated and the appropriate parameter choices. In the creep experiments with relatively high sustained loads the role of the cracking velocity becomes crucial for the prediction of the time to failure, as well as the deformation at which failure occurs.

The geometry of the 100 mm thick notched concrete beams, which were tested by Zhou (1992), is shown in Fig. 7. The beams were sealed to avoid shrinkage. The experimental displacement-controlled results and creep results are shown in Fig. 8. For the former experiments, both the load versus the crack mouth opening displacement (CMOD) and the load versus the deflection at midspan are shown. The deflection rate was

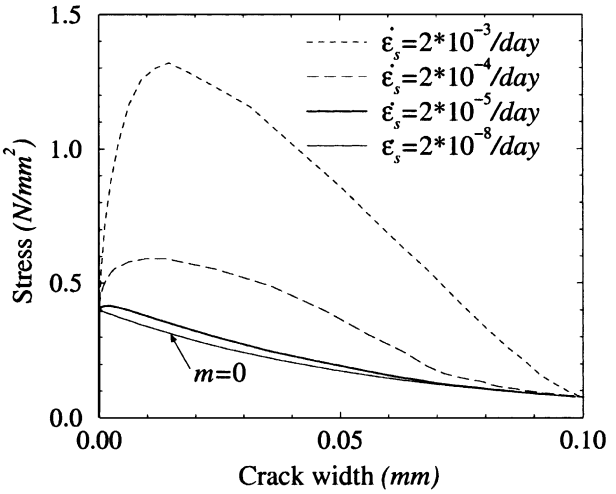

Fig. 5. The mechanical response of uniaxially restrained masonry subjected to various, constant shrinkage rates for $m = 2000$ N day mm^{-2}.

5 μm s^{-1}. For the creep tests the central force was increased gradually to a predefined level and subsequently sustained. Creep tests were performed at 76%, 80%, 85% and 92% of the peak resistance obtained in the displacement-controlled experiments. In each case failure eventually occurred, indicated by an X in Fig. 8. The displacement-controlled response seems to form a failure envelope, which determines the deformation at failure under the sustained load.

The finite element mesh employed for the analyses is also shown in Fig. 7. It consists of plane-stress, four-noded quadrilateral elements. Symmetry is exploited, enabling only one half of the beam to be modelled. A crack bandwidth $l_b = 4$ mm is assumed, which is equal to the notch width. The own weight is compensated for by applying a volume load of mass density 2400 kg m^{-3} in an initial step in each analysis.

5.1. Characterisation of the model parameters

Separate tests were performed to characterise the material, yielding a Young's modulus 36 kN mm^{-2} and a tensile strength $f_t = 2.8$ N mm^{-2} (Zhou, 1992). Also, relaxation tests were performed on cylindrical, notched tensile specimens, providing information for determining the bulk creep parameters (Fig. 9). Unfortunately, the relaxation was measured over short times (maximum 1 h), calling for extrapolation. Two such extrapolations were made to give creep coefficients of $\phi = \varepsilon_c/\varepsilon_e = 2$ and 5 respectively after 100 days, considered to be the limiting cases for concrete. A 10-element Maxwell chain model was fitted by a least squares method to each relaxation curve (Fig. 9). The initial load on the specimens was about 75% of the strength, so inevitably micro-cracking must have occurred and influenced the amount of relaxation, but this is ignored here.

Zhou (1992) also performed three-point bending tests under displacement control on smaller beams (600 mm long by 50 × 50 mm^2 section) to determine the fracture energy G_f. By varying the deflection rate from slow (0.05 μm s^{-1} – peak load after about 80 min) to fast (50 μm s^{-1} – peak load after about 5 s) he studied the rate influence on the fracture energy (Fig. 10a) and peak strength (Fig. 10b).

The same loading rate experiments enable the determination of the CMOR parameters, albeit in an indirect way from the analysis of these experiments and a process of inverse fitting of the parameters in Eqs. (13) and (14). The smaller beam has been modelled with the same mesh shown in Fig. 7, scaled to the small

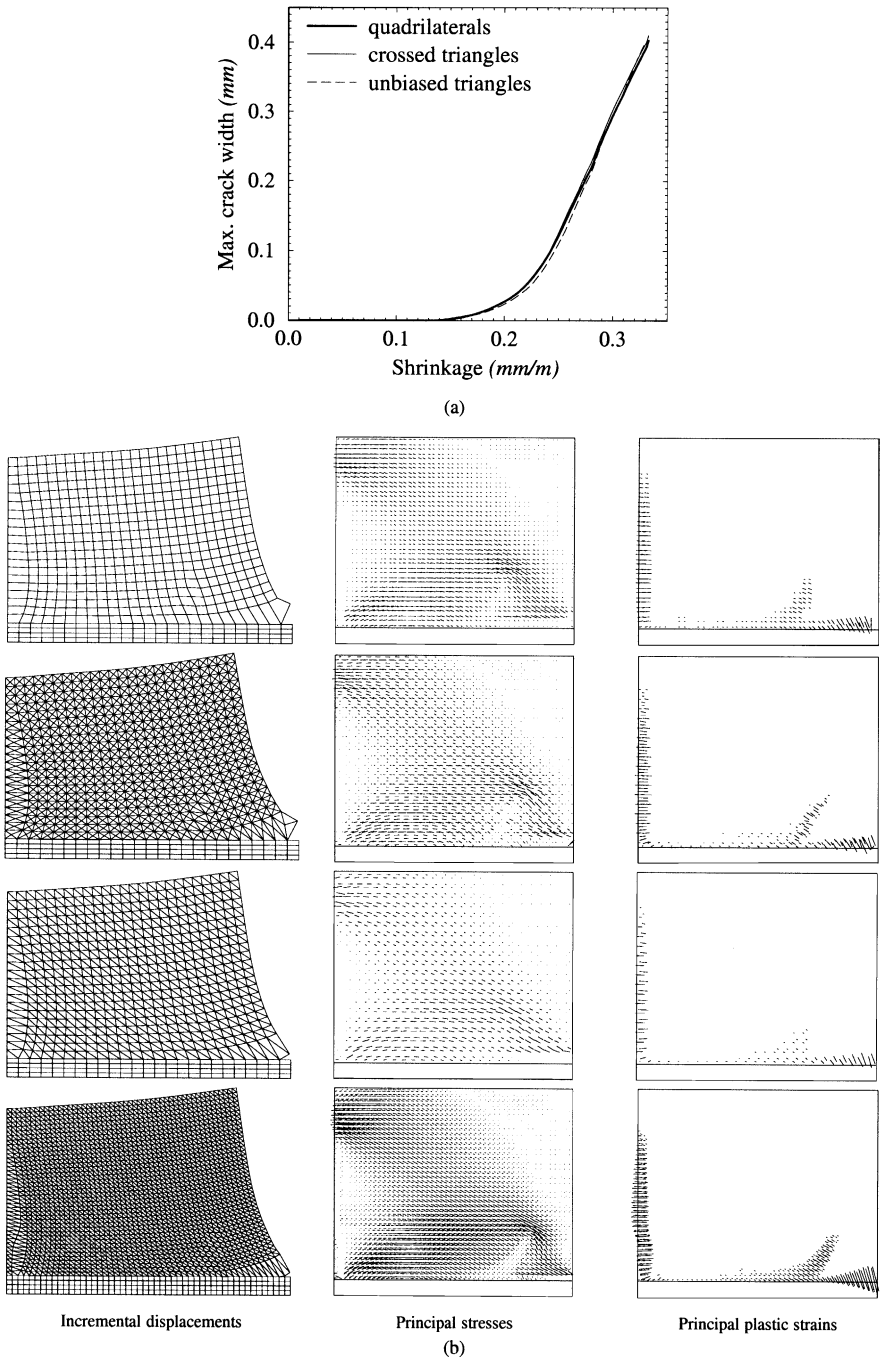

Fig. 6. Regularised base-restrained shrinking masonry wall response. (a) Primary crack width evolution. (b) Deformation, maximum principal stresses and principal plastic strains.

beam geometry. The parameters which have been obtained in this way are, for Eq. (13): $k_0 = 0.05$, $k_1 = 0.1$, $\dot{\kappa}_r = 10^{-7}\ s^{-1}$ and for Eq. (14): $m = 1500\ N\,s\,mm^{-2}$. In Fig. 10b the normalised numerical peak strengths are

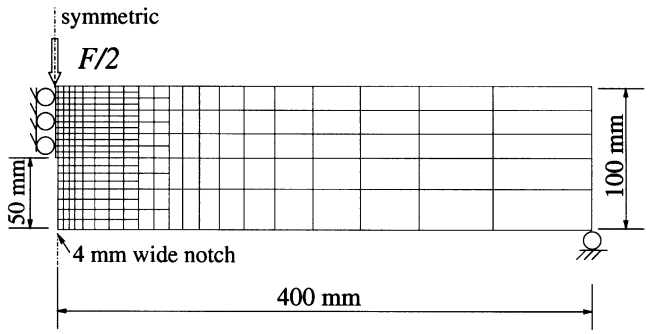

Fig. 7. Three-point bending tests by Zhou (1992): Specimen geometry, set-up and FE model.

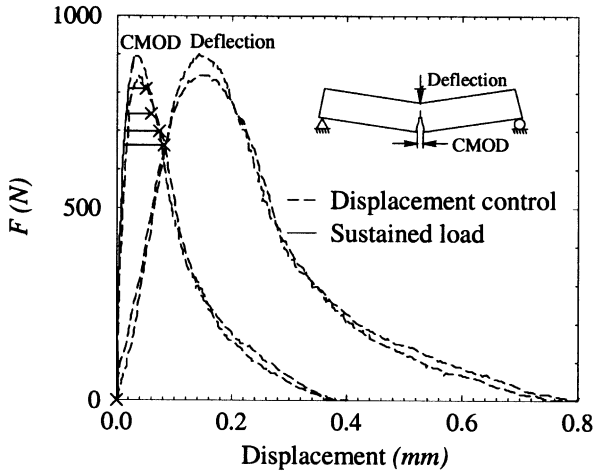

Fig. 8. Experimental three-point bending test responses (Zhou, 1992).

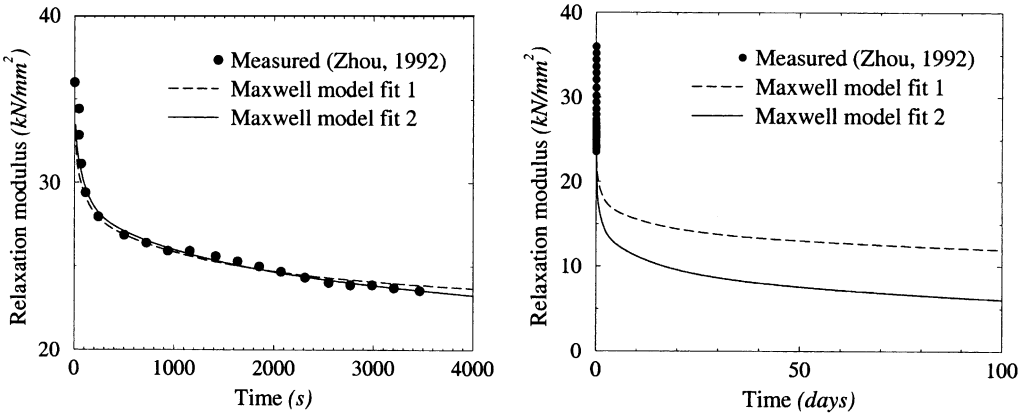

Fig. 9. Maxwell chain fits to the extrapolated relaxation data.

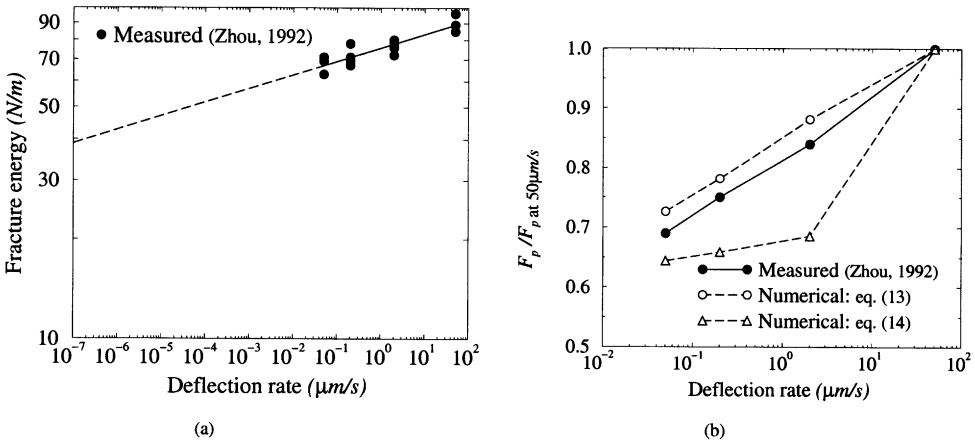

Fig. 10. Rate effect on (a) fracture energy and (b) peak strength in three-point bending tests.

compared with the measured values. Reasonable agreement is found with the three-parameter model, but with the simple one-parameter model it is impossible to fit the strength increase over the entire range of loading rates. A possible remedy is to employ a rate-dependent viscosity $m(\dot{\kappa})$. This has not been attempted. Instead, the three-parameter model (Eq. (2)) has been employed for the subsequent analyses in this study.

With regard to the apparent increase in fracture energy with loading rate, it must be noted that it follows from the numerical model while employing a prescribed constant fracture energy. This value can be estimated by extrapolation to the deflection rate at the reference crack mouth opening strain rate $\dot{\kappa}_r$ (Fig. 10a). A constant value of $G_f = 35\ \mathrm{N\,m^{-1}}$ has been used.

5.2. The response with bulk creep and CMOR activated

The displacement-controlled case is analysed first, with the deflection rate 5 $\mu\mathrm{m\,s^{-1}}$, as employed in the experiment. Note that the Maxwell model fit 2 (Fig. 9) is employed. Fig. 11 compares the numerical re-

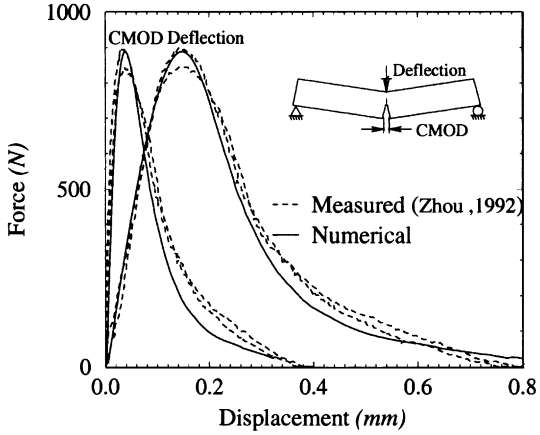

Fig. 11. Displacement-controlled (5 $\mu\mathrm{m\,s^{-1}}$) experimental and numerical force–deflection and force–CMOD responses.

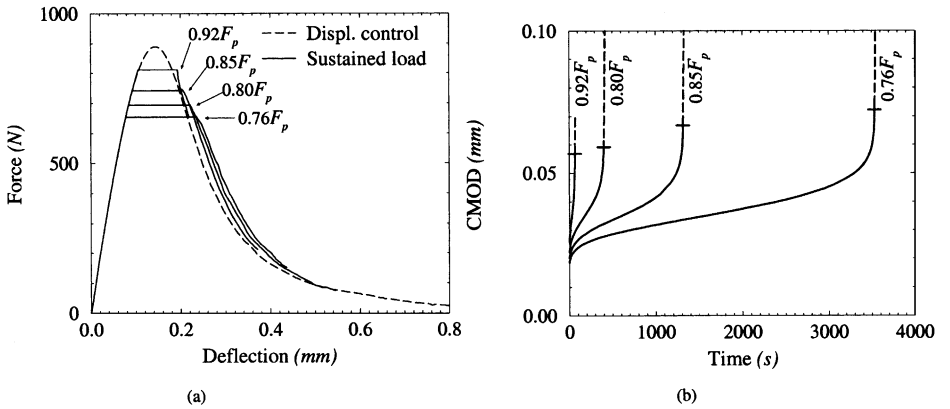

Fig. 12. Three-point bending numerical results. (a) Force–deflection responses and (b) CMOD evolutions.

sponse with the experimental responses. To obtain this agreement a 5% lower tensile strength than the reported $f_t = 2.8\ \mathrm{N\,mm^{-2}}$ (Zhou, 1992) and a Young's modulus 30 $\mathrm{kN\,mm^{-2}}$ have been used. On the one hand these adjustments have been made to give reasonable agreement with the experimental responses, in order to make possible the subsequent comparison between the responses under sustained load. On the other hand the strength and stiffness are rate dependent. Thus, the reduction of the measured parameters is in line with the determination of the "rate-independent" values, as has been done in the previous section for the fracture energy.

Next, the sustained load cases are analysed. As for the displacement-controlled analyses of the previous section, the Maxwell model fit 2 is employed. Fig. 12 shows the results. Following the experiments (Zhou, 1992), the load is increased to a certain portion of the peak load F_p of the displacement-controlled analysis. Four cases are considered, namely load levels of $0.76F_\mathrm{p}$, $0.80F_\mathrm{p}$, $0.85F_\mathrm{p}$ and $0.92F_\mathrm{p}$. As was attempted in the experiments, the initial, ascending loading rate is the same as for the displacement-controlled case. Beyond this ascending branch the load level is kept constant and the creep behaviour is analysed. During this stage the crack propagates and the deflection and CMOD increase up to a point where equilibrium can no longer be achieved for the sustained load level. Here, the load bearing capacity of the beam is exceeded. To ensure that failure under the sustained load is indeed imminent, the analyses are continued, by replacing the force control with displacement control at this point. This results in the subsequent softening responses (Fig. 12a) which prove that failure would have occurred under continued load control. The CMOD evolutions are shown in Fig. 12b. The points of failure are marked, with dashed lines indicating the subsequent continued crack mouth opening under displacement control.

These results confirm the experimental observation that the displacement-controlled response serves as an envelope for failure under sustained loads. Also, reasonable agreement is found with the measured times between reaching the sustained load level and failure t_f (Fig. 13). The agreement between the measured and computed CMOD values at the point of failure, marked in Fig. 12b, is reasonable. This is quantified in Table 1.

5.3. The response with only bulk creep activated

To investigate the role of the CMOR dependence by a process of elimination, it is deactivated and the analyses of the Zhou experiments are repeated. Once again the Maxwell model fit 2 (Fig. 9) is employed to capture the bulk creep, which is now the only numerical source of time dependence. For these crack rate-independent analyses the model parameters applicable at the 5 $\mu\mathrm{m\,s^{-1}}$ loading rate, namely $G_f = 80\ \mathrm{N\,m^{-1}}$,

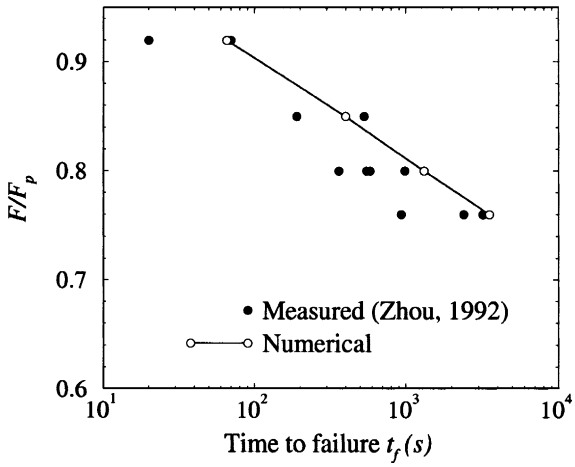

Fig. 13. Time to failure of three-point bending creep specimens.

Table 1
CMOD at the point of failure of three-point bending creep specimens

F/F_p	0.92	0.85	0.80	0.76
Measured CMOD (μm): (Zhou, 1992)	48	57	70	77
Numerical (μm):	56	59	67	72

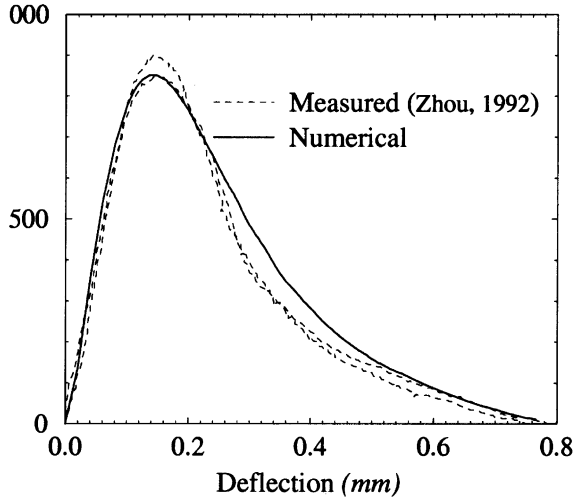

Fig. 14. Displacement-controlled (5 $\mu m s^{-1}$) experimental and numerical force–deflection responses when the CMOR dependence is deactivated in the analysis.

$f_t = 2.8\ N mm^{-2}$ and $E = 36\ kN mm^{-2}$, are employed. This is done to obtain agreement with the measured behaviour under displacement control (Fig. 14) to allow subsequent comparison of the experimental and numerical sustained load responses.

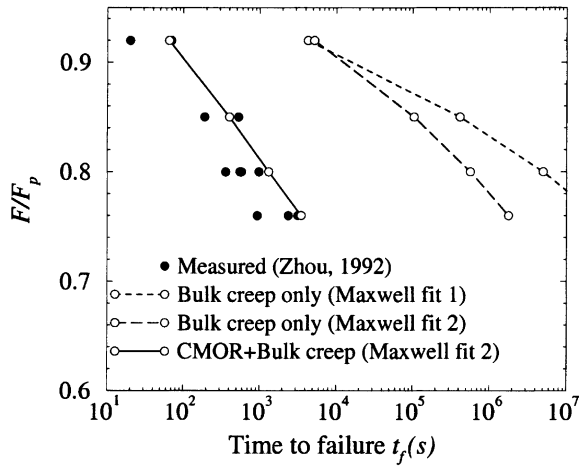

Fig. 15. Comparison of measured and computed times to failure of three-point bending beams under sustained loads.

Subsequently, the creep analyses are repeated. Fig. 15 shows that the time to failure is greatly overestimated if only bulk creep is considered. The creep analyses have also been performed with the Maxwell model fit 1 (Fig. 9) to assess the failure speed-up possible by employing the extreme relaxation moduli. It is clear that there is no way that bulk creep can capture the correct time scale. The CMOR contribution is significant in the Zhou experiments, because if it is ignored in the analyses, the predicted time to failure under the sustained loads are overestimated by several orders of magnitude.

Another issue worth investigating is the contradiction between the failure envelope of the Zhou creep experiments (Fig. 12a) and the failure envelope by Rüsch (1960) (Fig. 16). To do so, the displacement-controlled analysis with only bulk creep activated is repeated for various deflection rates, with times to peak 30 s (the 5 $\mu m s^{-1}$ case), 10 h, 75 days and several years respectively (Fig. 17a). The numerical creep responses with only bulk creep activated are also shown in this figure. The X symbols denote the points after which no further convergence can be found under the sustained load, which indicates a reduced load carrying capacity and thus failure. The vertical slope of the CMOD responses shown in Fig. 17b confirms that failure is due in each case. A larger deformability before failure is now found than Zhou observed and, as reported by Rüsch, the failure envelope is now formed roughly by the connection of the short-term and long-term load–deformation responses. It can be argued that Fig. 17a confirms the failure envelope by

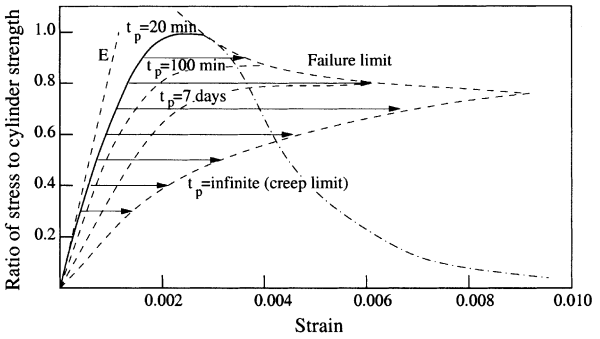

Fig. 16. Influence of load intensity and duration on concrete strain (Rüsch, 1960; reprinted with kind permission of the ACI).

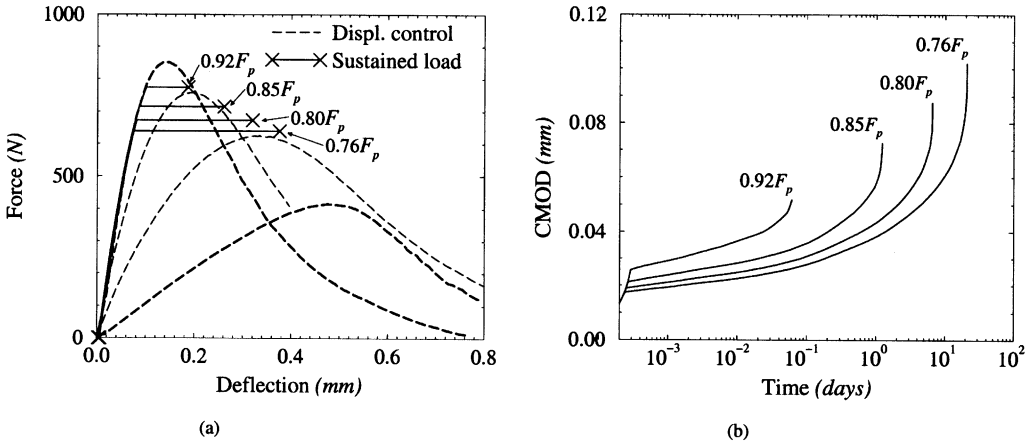

Fig. 17. Numerical three-point bending results with only bulk creep considered: (a) force–deflection responses for various constant deflection rates and various creep load levels, (b) CMOD evolutions under sustained load.

Rüsch for cases where the CMOR dependence is negligible, for instance in concrete compressive tests, where more diffuse (splitting tensile) cracking occurs.

6. Discussion and conclusions

Evidence has been presented that the inclusion of (a) rate term(s) in the description of quasi-static crack initiation and propagation in cementitious materials is not merely a numerical artefact. Not only does it capture the rate-dependent global strength, but it also introduces the true time scale in crack propagation. This enables the prediction of life expectancy under mechanical action, an important aspect in the consideration of structural durability.

The regularisation by visco-plastic models is well known. Here it has been shown that the presented rate-dependent visco-elastic softening plastic model does not only predict the crack orientation independent of finite element discretisation, but also objectively predicts crack spacing in large scale masonry walls.

The indirect way of characterisation of the crack rate model parameters to "fit" the experimental increase in resistance with increasing loading rate remains a drawback. However, this is in line with the characterisation of most creep models and ascribed to the fact that the micro-structural mechanisms are not yet properly understood. Due to lack of characterisation data, the cracking viscosity which modifies the uniaxial cracking stress "sufficiently" under the prescribed hygral shrinkage in the masonry wall analyses was chosen. Hereby, a value was obtained, which is of the same order of that of the low viscosity Maxwell chain element ($m = 2000\ \mathrm{N\,day\,mm^{-2}}$, $\eta_1 = E_1\zeta_1 = 840\ \mathrm{N\,day\,mm^{-2}}$). This also holds for the second case study, ($m = 1500\ \mathrm{N\,s\,mm^{-2}}$, $\eta_1 = 500\ \mathrm{N\,s\,mm^{-2}}$). Unfortunately, the Maxwell chain parameters cannot be uniquely obtained. This suggests a correlation between the cracking viscosity and the Maxwell dash-pot viscosities, a subject for further investigation.

Another aspect for further investigation is the correct description of the physical aspects of rate dependence over the entire range of quasi-static rates, while maintaining the ability to regularise. The three-parameter model succeeds in capturing the strength increase reasonably, but has been shown to regularise for only a limited range of rates due to the strong inverse hyperbolic operator. The one-parameter, constant cracking viscosity model overestimates the strength increase for a substantial increase in loading rate. A possible remedy is a varying, rate-dependent cracking viscosity.

Acknowledgements

The authors gratefully acknowledge the financial support by the Netherlands Technology Foundation (STW) under the grant DCT 44.3406.

References

Bažant, Z.P., Chern, J.C., 1985. Concrete creep at variable humidity. Materials and Structures 18 (103), 1–20.
Bažant, Z.P., Gettu, R., 1992. Rate effects and load relaxation in static fracture of concrete. ACI Materials Journal 89 (5), 456–468.
Bažant, Z.P., Oh, B.H., 1983. Crack band theory for fracture of concrete. Materials and Structures 16 (93), 155–177.
Bažant, Z.P., Xiang, Y., 1997. Crack growth and lifetime of concrete under long time loading. Journal of Engineering Mechanics 123, 350–358.
de Borst, R., Feenstra, P.H., Pamin, J., Sluys, L.J., 1994. Some current issues in computational mechanics of concrete. In: Mang, H., et al. (Eds.), Computational Modelling of Concrete Structures. Pineridge Press, Sansea, UK, pp. 283–302.
de Borst, R., van den Boogaard, A.H., Sluys, L.J., van den Bogert, P.A.J., 1993. Computational issues in time-dependent deformation and fracture in concrete. Creep and Shrinkage of Concrete. E&FN Spon, London, pp. 309–325.
Feenstra, P.H., 1993. Computational aspects of biaxial stress in plain and reinforced concrete. Dissertation, Delft University of Technology, Delft, The Netherlands.
Lourenço, P.B., 1996. Computational strategies for masonry structures. Dissertation, Delft University of Technology, Delft, The Netherlands.
Powers, T.C., 1968. Mechanism of shrinkage and reversible creep of hardened cement paste. International conference on the structure of concrete. Cement and Concrete Association, London, pp. 319–344.
Rots, J.G., 1997. Structural masonry; an experimental/numerical basis for practical design rules. Balkema, Rotterdam.
Rüsch, H., 1960. Researches toward a general flexural theory for structural concrete. ACI Journal 57 (1), 1–28.
Shrive, N.G., Sayed-Ahmed, E.Y., Tilleman, D., 1997. Creep analysis of clay masonry assemblages. Canadian Journal of Civil Engineering 24 (3), 367–379.
Sluys, L.J., 1992. Wave propagation, localisation and dispersion in softening solids. Dissertation, Delft University of Technology, Delft, The Netherlands.
van der Pluijm, R., Wubs, A.J., 1996. The time dependent deformational behaviour of masonry. Report 96-CON-R0901-02, TNO Building and Construction, Delft, The Netherlands (in Dutch).
van Zijl, G.P.A.G., 2000. Computational modelling of masonry creep and shrinkage. Dissertation, Delft University of Technology, Delft, The Netherlands.
Wang, W., 1997. Stationary and propagative instabilities in metals – a computational point of view. Dissertation, Delft University of Technology, Delft, The Netherlands.
Wu, Z.S., Bažant, Z.P., 1993. Finite element modelling of rate effect in concrete fracture with influence of creep. In: Bažant, Z.P., Carol, I. (Eds.), Creep and Shrinkage of Concrete E&FN Spon, London, pp. 427–432.
Zhou, F.P., 1992. Time-dependent crack growth and fracture in concrete. Dissertation, Lund University, Lund, Sweden.